Chapter 4: Results and discussion

As mentioned in Chapter 3, composite films of untreated/ pre-treated banana fiber and PVA were prepared and characterized. Pre-treatment was done using aqueous acid and alkali solutions. Various additives such as glutaraldehyde, glycerol, sorbitol, fructose, citric acid, and maleic acid were used to improve the mechanical strength and water absorption properties. The glutaraldehyde served as the primary cross-linker and citric and maleic acids as the second cross-linker. Fructose, glycerol, and sorbitol acted as plasticizers. The nanocellulose prepared from microcrystalline cellulose was used to improve the barrier properties and mechanical strength of PVA- BPF composite films. In another batch of PVA-BPF composite films, citric acid treated and un-treated montmorillonite clay were used in place of nanocellulose, and properties were tested. The results obtained for various types of films thus prepared are discussed and presented in this chapter.

4.1: Optimization of Film preparation

The PVA- BPF composite films were prepared using the solution casting method. The primary and secondary cross-linkers such as glutaraldehyde and citric acid/ maleic acid, respectively, improved the mechanical strength and water-resistant properties. The plasticizers like glycerol, sorbitol, and fructose improved the film-forming ability and flexibility of films. Effects of chemical nature and concentration of these additives were investigated to get an optimal formulation to prepare the composite films having desired characteristics. The banana pseudostem fibers of different lengths (75-90, 53-75, and <53μm) and various ratios of PVA: BPF by weight (90-10, 80-20, 70-30, and 60-40) were used to come out with the best size and composition.

Effects of the amount and size of BPF in the PVA-BPF mixture, amount of glutaraldehyde, chemical nature, amount of plasticizer, and amount of second cross-linker (citric or maleic acid) are discussed and presented in the following sections.

4.1.1 Effect of BPF size and ratio

The banana pseudostem fibers in size range of <53, 53-75, and 75-90 μm were used to prepare different casting solutions having PVA: BPF ratios of 100:0, 90:10, 80:20, 70:30, and 60:40. No cross-linker and plasticizer were used. **Table 4.1** lists the values of tensile strength (MPa) and percent elongation for the films of different PVA: BPF ratio and different fiber size. **Figures 4.1** and **4.2** show the comparison of the tensile strength and percent elongation at break-point, respectively for PVA-BPF composite films with different ratio and fiber size..

Effect of fiber size

From **Figures 4.1** and **4.2** and **Table 4.1**, it is seen that the best values of tensile strength and percent elongation at break-point are exhibited by the films made with the smallest fiber(<53 μm). It is seen that at 10% loading of BPF, the increase in fiber size from <53 μm to 75-90 μm range results in a decrease in the tensile strength by 29.4% and elongation at break-point by 19.3 %. This trend of reduction in tensile strength and percent elongation at break-point is exhibited by films made with higher loadings of BPF. The reduction in tensile strength is 17.9, 22.8, and 31.5% and that in percent elongation at break-point are 27, 35.2, and 45.4% for 20, 30, and 40% loadings of BPF, respectively.

The smaller fibers have a higher surface area to volume ratio compared to larger ones. These are more uniformly dispersible in the casting solution leading to the formation of a more homogenous film. Further, more hydrogen bonds may form between the fibers

and PVA polymer chains due to the higher surface area to volume ratio. These result in an increased matrix – fiber adhesion and hence improved mechanical properties. The surface morphology of the films formed with larger fiber particles was observed to be relatively rough. The larger fiber particles exhibited the tendency of agglomerating due to cohesive and van der Waal type forces. These fiber agglomerates do not permit uniform distribution of BPF in PVA solution leading to reduced fiber-polymer interactions, hence poor mechanical strength.

Effect of fiber loading

Effect of fiber loading was investigated by varying the amount of <53 μm fibers in PVA-BPF mixture as 10, 20, 30, 40%. The tensile strength (MPa), percent elongation at break-point, water vapor permeability (g.m/m^2.s.Pa), and contact angle (^{o}) were determined in each case. These results are listed in **Table 4.2** and depicted in **Fig. 4.3** and **4.4**.

Table 4.1: Effect of PVA: BPF ratio and fiber size on tensile strength and elongation at break-point %

	Tensile Strength, MPa			Elongation at break, %		
PVA : BPF ratio	**<53 μm**	**53-75 μm**	**75-90 μm**	**<53 μm**	**53-75 μm**	**75-90 μm**
100 : 0	31.7±2.3	31.7±2.3	31.7±2.3	183.4±16.1	183.4±16.1	183.4±16.1
90:10	30.3±2.6	28.5±3.4	21.4±2.4	113.7±11.3	100.5±10.4	91.7±8.9
80 : 20	30.8±2.4	27.6 ±1.9	25.3 ±2.3	68.93±5.7	57.2±7.6	50.3±6.1
70 : 30	14.5±3.1	13.9 ±1.2	11.2 ±1.4	38.74±5.3	32.7±7.4	25.1±7.6
60 : 40	12.7±2.3	10.8 ±1.1	8.7±1.2	37.29±6.1	29.4±5.6	20.36±4.7

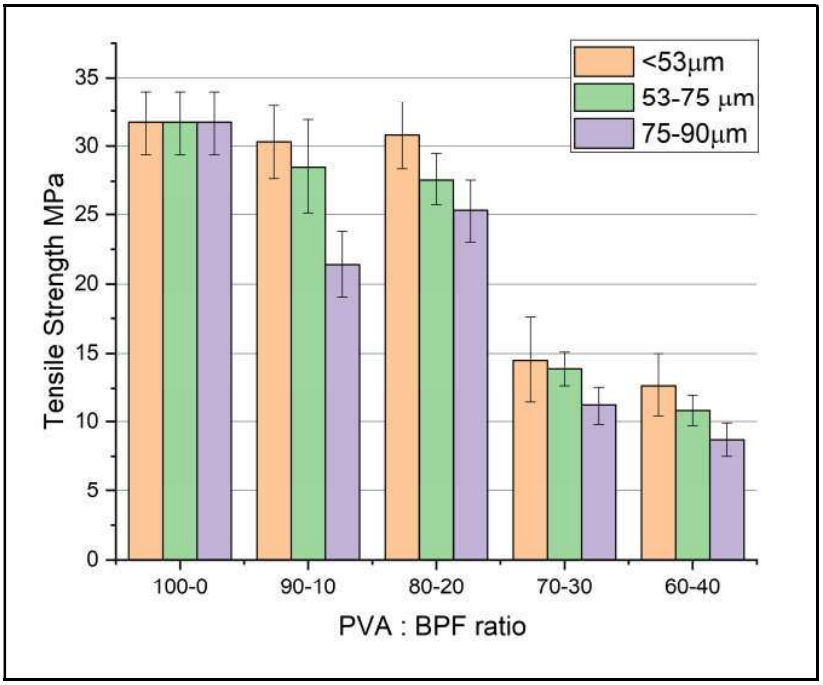

Figure 4.1: Variation of tensile strength of PVA-BPF composite films with fiber size and PVA: BPF ratio

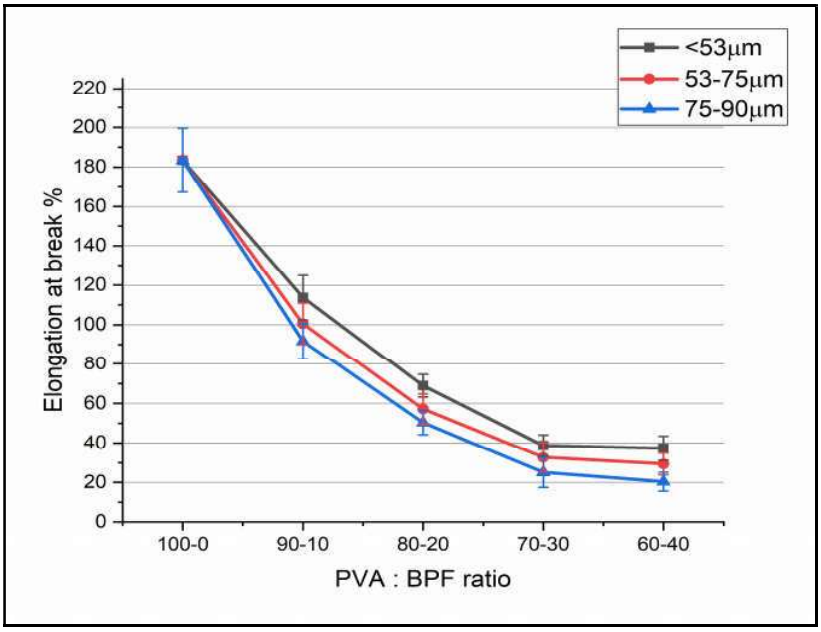

Figure 4.2: Variation of percent elongation of PVA-BPF composite films with fiber size and PVA: BPF ratio

From **Table 4.2** and **Fig. 4.3**, it is seen that the percent elongation at break-point decreases monotonously up to BPF loading of 30% and there after it becomes nearly

constant. **Fig. A1 (a) and (b)** show the stress vs. strain curves for PVA and PVA-BPF composite films. The tensile strength similarly exhibits a decreasing trend with fiber loading however the decrease is marginal up to 20 % fiber loading after which it decreases drastically. BPF loading in PVA matrix results in composites with higher mechanical strength due to hydrogen bonding between hydroxyl groups present on PVA matrix and on BPF (Sathasivam et al., 2010; Solikhin et al., 2018; Yang et al., 2009). With increase in fiber loading, the higher availability of BPF in the casting solution tends to form agglomerates leading to discontinuities in the film structure. These discontinuous regions affect the load bearing ability of the films and they tend to have lesser tensile strength and elongation at break-point (Sathasivam et al., 2010; Yang et al., 2009)

Figure 4.4 shows water vapour permeability of composite films. It is seen that the water vapor permeability of the PVA-BPF composite films gradually increases, i.e. hydrophillicity gradually increases with increasing loading of BPF. The BPF in itself is hydrophilic and its incorporation into PVA matrix further increases the hydrophillicity of composite films.

Table 4.2: Effect of BPF loading on tensile strength, elongation at breakpoint, water vapor permeation and water contact angle for various films prepared with <53µm fibers

PVA : BPF ratio	Tensile Strength (MPa)	Elongation at Break-point (%)	WVP ($x10^{-10}$g.m / m^2.s. Pa)	Contact Angle (°)
100 : 0	31.7±2.3	183.4±16.1	1.53±0.35	65.8
90:10	31.3±2.7	113.7±14.5	2.19±0.52	66.4
80 : 20	**30.8±1.8**	**68.9±14.2**	**2.57±0.35**	**67.2**
70 : 30	22.7±2.2	38.7±10.9	3.22±0.7	56.3
60 : 40	17.5±1.4	37.3±10.6	3.71±0.52	51.7

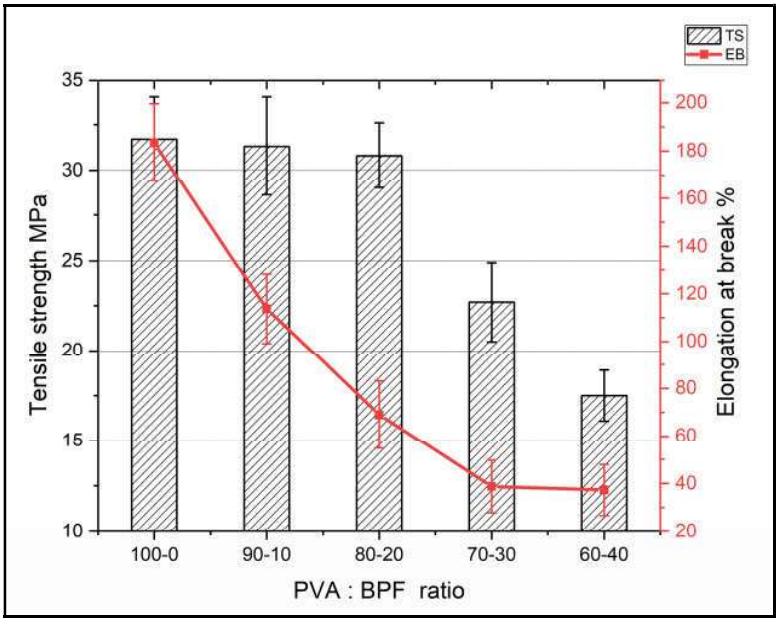

Figure 4.3: Variation of tensile strength and percent elongation at break-point with BPF loading (fiber size <53µm)

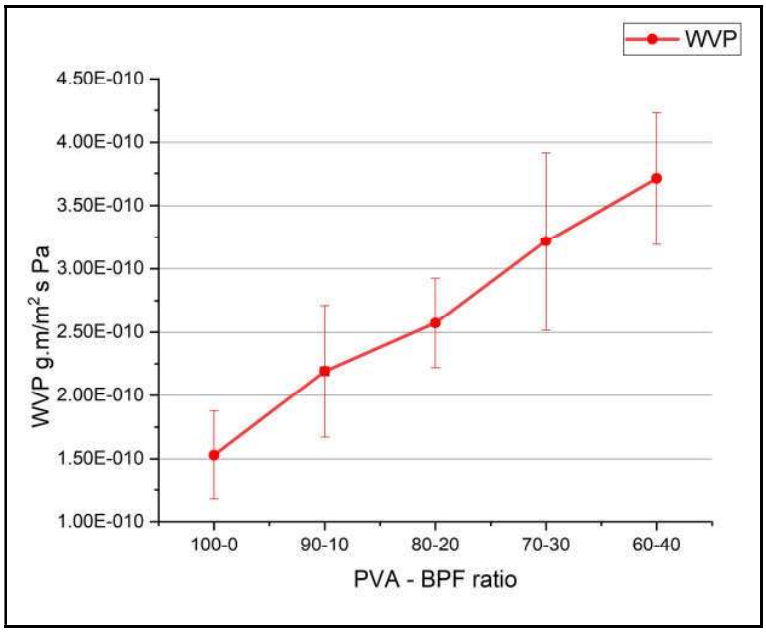

Figure 4.4: Variation of water vapor permeation with BPF loading (fiber size <53µm)

4.1.2 Effect of cross linker

Cross linkers are used to improve flexibility, tensile strength and other properties of films. The PVA films and membranes have long been cross-linked with various molecules (known as cross-linkers) to improve their physical and chemical properties. Cross-linkers like glutaraldehyde, urea - formaldehyde, citric acid, maleic acid etc have been used with the intention of improving the mechanical strength of films. In the present work glutaraldehyde has been used as the primary cross-linker due to its widespread use as a cross-linker for PVA and presence of two aldehyde groups which effectively crosslink the PVA polymer chains. However, a fine balance should be maintained in using glutaraldehyde since above a particular concentration the glutaraldehyde can cause formation of branches instead of cross linking the polymer chains. As shown in **Figure 4.5**, glutaraldehyde reacts with PVA polymer in two different ways. It can crosslink two polymer chains and if present in excess, it can promote branching of PVA chains (Yeom and Lee, 1996). The cross-linking of polymer chains results in films of higher tensile strength but the elasticity gets reduced as the polymer chains are cross-linked into a tight structure. Further the cross-linking increases tortuosity thereby hampering the diffusion of water vapor leading to lower WVP values. If branching occurs due to excess glutaraldehyde, the network structure so formed will no longer be tightly bound and WVP values get elevated with slight effect on mechanical properties also (Figueiredo et al., 2009).

Table 4.3 presents the variation of tensile strength, percent elongation at breakpoint, water vapor permeability and water contact angle with increasing amount of glutaraldehyde. As seen from **Fig. 4.6**, with increase in glutaraldehyde concentration from 0.1 to 2 wt %, the tensile strength linearly increases from 32.4 to 38.3 MPa and the percent elongation at break-point decreases from 91.6 to 54.2%. Similar results have

been reported by (Priya et al., 2014b; Yoon et al., 2006). **Fig. A1 (c)** shows the stress vs. strain curves for PVA-BPF composite films with glutaraldehyde.

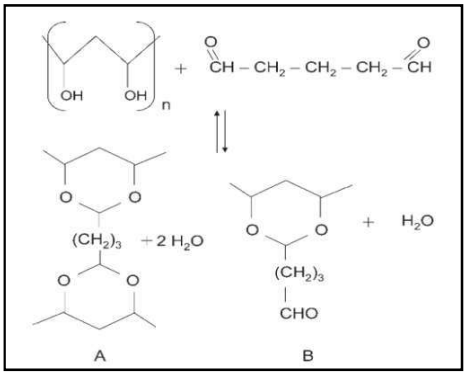

Fig. 4.5 Reaction of glutaraldehyde with PVA

Higher concentration of glutaraldehyde results in stiffer films with great strength and reduced elasticity. The water vapor permeability is also affected by the addition of glutaraldehyde. By increasing glutaraldehyde amount from 0.1 to 2 wt % the WVP value decreases from 2.19x 10^{-10} to 1.63 x 10^{-10} g m/s m^2 Pa (**Fig. 4.7**). From these results it is clear that the cross-linking of glutaraldehyde with PVA-BPF composite films was successful in significantly improving the overall hydrophillicity of films as evident from the lowering of the water vapour permeability, water swelling of films and increase of water contact angle.

The PVA-BPF composite films without glutaraldehyde dissolved in water within first 24 hours only. As seen in **Fig. 4.8** the films made with various amounts of glutaraldehyde (0.1 to 2.0%) as cross-linker were not only more resistant to dissolution in water but also reduced the water swelling from 81% (at 0.1wt %) to 29% (at 2 wt% loading). Similarly water contact angle also increased from 71.3° for PVA-BPF composite film to 79.2° for PVA-BPF film having 2 wt% glutaraldehyde as the cross linker. These results further support the increase in hydrophobicity of films due to the

reaction of hydroxyl groups of PVA with aldehyde groups of glutaraldehyde (Priya et al., 2014a).

In view of the good mechanical properties and water resistance, 1% of glutaraldehyde cross-liker was considered as satisfactory.

Table 4.3: Effect of glutaraldehyde concentration on tensile strength, percent elongation at break-point, water vapor pressure and contact angle of PVA – BPF composite films

Glutaraldehyde wt %	Tensile Strength (MPa)	Elongation at Break-point (%)	WVP ($x10^{-10}$g.m / m^2.s. Pa)	Contact Angle (°)
0	30.8±1.8	68.9±14.2	2.57±0.35	67.2
0.1	32.4±2.2	91.6±11.8	2.19±0.4	71.3
0.5	33.7±2.5	87.3±9.9	2.14±0.5	72.8
1	35.5±2.4	77.4±9.2	2±0.4	74.6
1.5	36.8±2.8	69.6±10.6	1.93±0.3	77.9
2	38.3±2.7	54.2±10.2	1.63±0.4	79.2

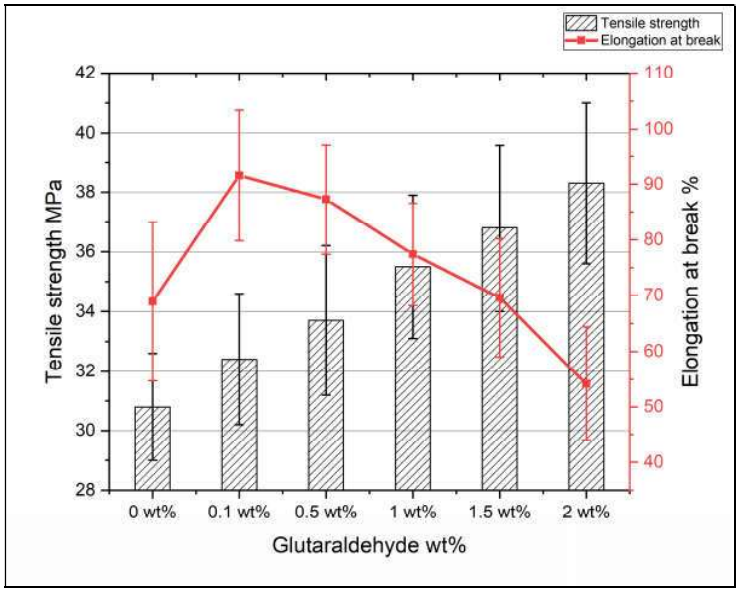

Figure 4.6: Variation of tensile strength and percent elongation at break-pointof PVA-BPF composite films: Effect of glutaraldehyde weight percent

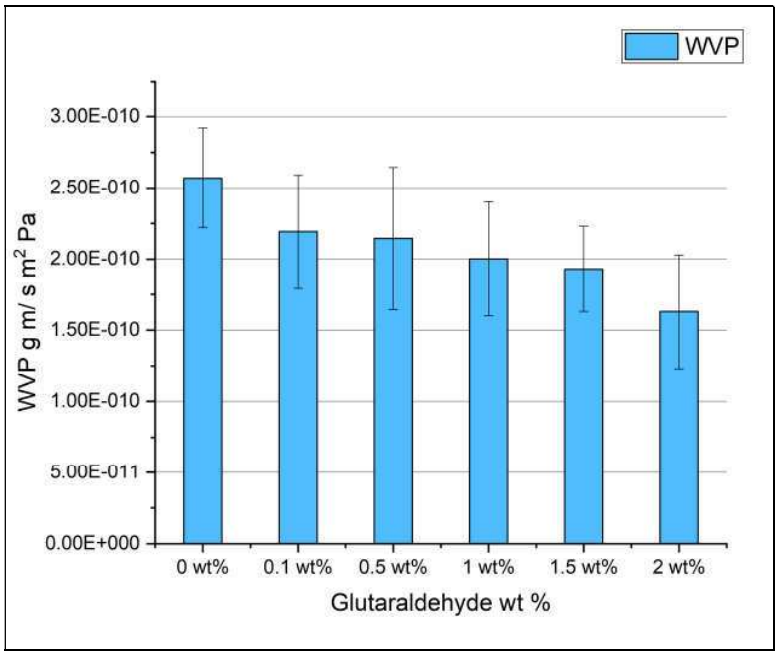

Figure 4.7: Variation of water vapor permeability of PVA-BPF composite films with glutaraldehyde weight percent

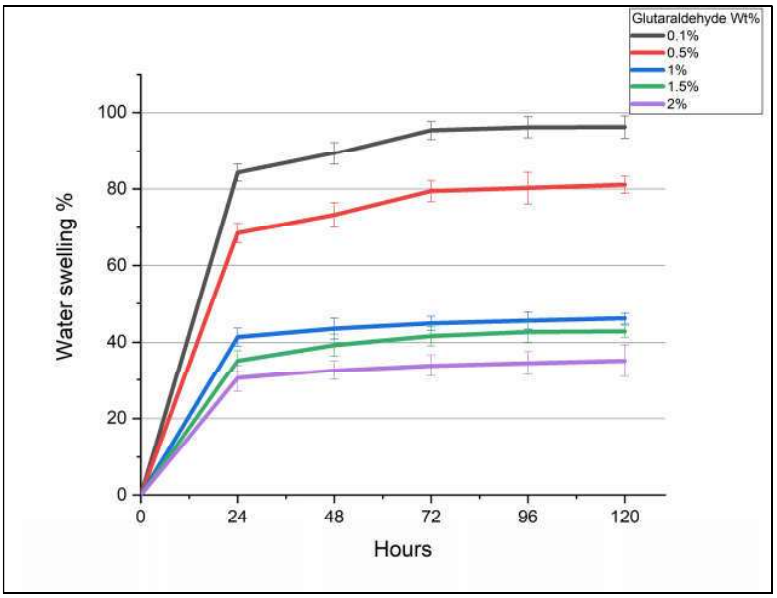

Figure 4.8: Variation of swelling in water of PVA-BPF composite films: Effect of glutaraldehyde weight percent

4.1.3 Effect of plasticizers

The addition of glutaraldehyde to PVA-BPF composite films considerably improved their tensile strength while decreased their percent elongation at break-point and stretchability. The cross-linking also improved swelling in water by reducing it to a fairly acceptable level. In order to further improve the stretchability of the films and make them more flexible, plasticizers were used. The plasticizers used belonged to the group polyols – glycerol, sugar alcohols - sorbitol and sugar - fructose. While glycerol is the most commonly used plasticizer (Cano et al., 2015; Chenwei et al., 2018a; Imam et al., 2005; Meng et al., 2018; More et al., 2019; W. Wang et al., 2018; Wu et al., 2017), sorbitol and fructose (Lusiana et al., 2019; Mohamed et al., 2018; Ooi et al., 2012) have also been reported to improve flexibility and therefore have been tested in the current work.

Five different concentrations (5, 10, 15, 20 and 25 wt %) of each plasticizer were used in PVA-BPF composite films cross-liked with glutaraldehyde. The experimental results for tensile strength, percent elongation at breakpoint, water vapor pressure and water contact angle are listed in **Table 4.4**.

For the 3 plasticizers used, the tensile strength decreased in the order- sorbitol > glycerol > fructose. The percent elongation at break-point and water vapor permeability also followed the same pattern. **Figure 4.9** and **4.10** show the variations of tensile strength and percent elongation at break-point with increasing amount of plasticizer in PVA-BPF composite films cross-linked with glutaraldehyde. **Fig. A1 (d), (e) and (f)** show the stress vs. strain curves for PVA-BPF composite films with glycerol, sorbitol and fructose plasticizer respectively. With increase in the plasticizer content from 5 to 25 wt%, the tensile strength reduced from 35.5 to 25.6, 22.08, and 16.5 MPa, respectively for sorbitol, glycerol, and fructose. The percent elongation at break-point

also got enhanced from 77.4% for unplasticized film and the values at 25 weight % of plasticizer were found to be 201.6, 187.6 and 192.6% for glycerol, sorbitol and fructose, respectively. These values are in accordance with the results reported by other investigators (Guimarães et al., 2015; Rouhi et al., 2017; Vieira et al., 2011). With increasing amount of plasticizers, the tensile strength gradually decreases and the percent elongation at the break-point gradually increases due to the intercalation of plasticizer molecules between the polymer chains causing increase in the mobility of the polymeric matrix. This increase in mobility however comes at the cost of decrease in the load transfer within the polymer – filler interface hence the tensile strength (Fajardo et al., 2016).

From **Figure 4.11** it is seen that the plasticizers tend to increase the water vapour permeability of the films. This can be attributed to the presence of hydroxyl groups on the plasticizer molecules which serve as water binding sites and increase the susceptibility of the film (Guimarães et al., 2015; Rouhi et al., 2017; Vieira et al., 2011) to water molecules. Since the molecular weight of glycerol sorbitol and fructose is around 92.09, 182.17 and 180.16 respectively, for the same weight percent of plasticizer added, we have twice the number of moles of glycerol than sorbitol or fructose. This may be the reason why glycerol causes **greater decrease in tensile strength and greater increase in elongation at break-point** than sorbitol or fructose.

The detrimental effect of plasticizer addition on Water vapour permeability of PVA-BPF composite films confers a limiting value upon the maximum wt% of plasticizers to be used. At 10 wt% loading sorbitol shows acceptable values of tensile strength, elongation at break-point and water vapour permeability. Any further increase in plasticizer content causes decline in the tensile strength and water vapour resistance therefore 10 wt% Sorbitol plasticizer loading was chosen to be the optimum for our

PVA-BPF cross-linked composite films as it exhibited the maximum tensile strength and minimum water vapour permeability among the plasticizers used and therefore it was selected as the plasticizer for preparing PVA-BPF composite films.

Table 4.4: Effect of plasticizer concentration and type on tensile strength, percent elongation at break-point, water vapor pressure and water contact angle of PVA – BPF composite films

	Tensile strength (MPa)			**Elongation at breakpoint (%)**		
Plasticizer %	Glycerol	Sorbitol	Fructose	Glycerol	Sorbitol	Fructose
0	30.8±1.8	30.8±1.8	30.8±1.8	68.9±14.2	68.9±14.2	68.9±14.2
5	32.8±2.7	35.7±2.2	30.1±2.5	103.7±10.7	96.33±18.1	99.8±11.9
10	30.2±2.8	32.6±2.9	29.3±3.4	113.6±13.7	105.33±13.1	108.4±11
15	28.5±2.5	30.3±2.3	27.1±2.5	138.7±12.7	124.86±17.1	130.86±8.6
20	25.7±2.8	28.4±2.7	19.4±1.5	184.3±14.9	150.5±12.9	165.5±12.2
25	22.08±1.6	25.6±2.9	16.5±2.3	201.6±17	187.6±9.6	192.6±16.9
	WVP ($x10^{-10}$ g.m/m^2/s/Pa)			**Water contact angle (°)**		
Plasticizer %	Glycerol	Sorbitol	Fructose	Glycerol	Sorbitol	Fructose
0	2.57±0.35	2.57±0.35	2.57±0.35	67.2	67.2	67.2
5	4.05±0.6	3.42±0.7	3.54±0.7	63.2	64.9	64.1
10	4.34±0.7	3.65±0.4	3.77±0.9	61.4	63.1	62.5
15	4.76±0.7	3.98±0.6	4.54±0.6	57.3	61.8	59.3
20	5.54±0.6	4.11±0.3	4.89±0.5	53.7	59.4	56.9
25	6.12±0.8	4.65±0.5	5.12±0.9	49.6	57.1	54.7

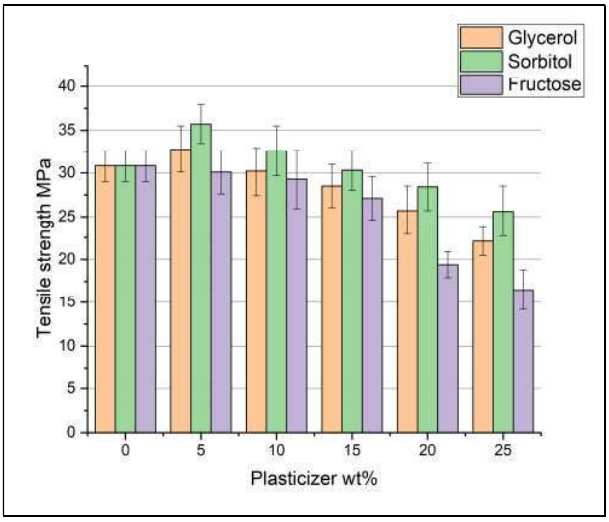

Figure 4.9: Variation of tensile strength of PVA-BPF composite films with the nature of plasticizer its weight percent

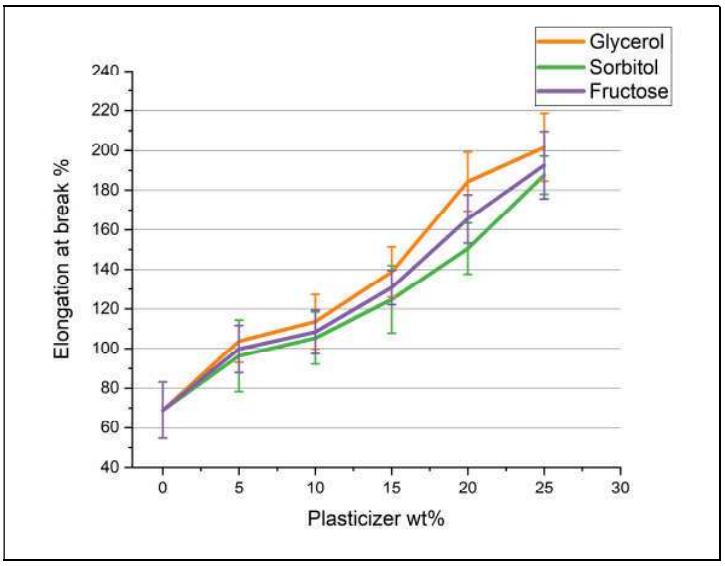

Figure 4.10: Variation of percent elongation at break-point of PVA-BPF composite films with the nature of plasticizer and its weight percent.

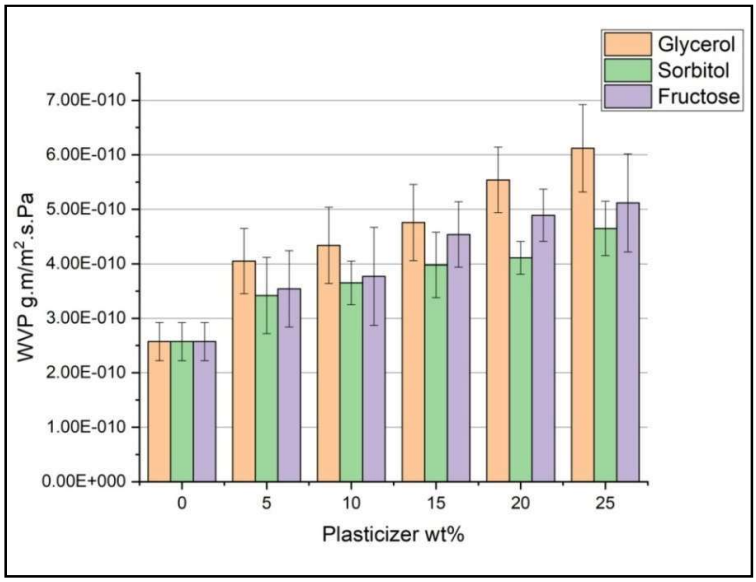

Figure 4.11: Variation of water vapor permeability of PVA-BPF composite films with the nature of different plasticizer and its weight percent

4.1.4 Effect of second cross-linker

After the selection of glutaraldehyde as the best cross-linker and sorbitol as the best plasticizer, experiments were performed to select a second cross-linker to further lower the WVP values and to increase the tensile strength of composite films.

Two related carboxylic acids- citric and maleic acids consisting of three and two carboxyl groups, respectively were used for this purpose: The number of carboxyl groups present on the cross-linker moiety directly affects its cross linking ability. **Figure 4.12** shows the effect of concentrations of citric and maleic acids on the tensile strength of PVA-BPF composite films and **Figure 4.13** shows their effects on percent elongation at the break-point. **Fig. A1 (g) and (h)** show the stress vs. strain curves for PVA-BPF composite films cross-linked with citric acid and maleic acid respectively. **Figure 4.14** shows the effect of concentrations of citric and maleic acids on WVP through PVA-BPF composite films. **Table 4.5** lists the weight % of two acids used as second cross-linkers in PVA-BPF films and their effects on the tensile strength, percent elongation at the break-point, water vapor permeation and water contact angle.

On increasing the CA or MA concentration from 5 to 25 wt% in PVA-BPF composite films, the tensile strength and percent elongation at the break-point are dramatically improved even after the addition of plasticizer. For citric acid an increase in the tensile strength is observed from 35.4MPa at 5 wt % loading to 38.3MPa at 10 wt% loading. Further loading of acid resulted in the reduction in the tensile strength and the percent elongation at the break-point was observed to increase from 91.11% at 5 wt % to 172.53% at 25 wt % acids. This can be attributed to the plasticizing effect of citric acid at higher concentrations, a common phenomenon reported by (Avella et al., 2000; Ghanbarzadeh et al., 2011; Yoon et al., 2006; Zou et al., 2008); and (Singha et al., 2015).

The effect of citric acid on water vapor permeation rate is also favorable up to 10 wt% and the PVA-BPF composite films showed the minimum WVP of $2.62x10^{-10}$ g m/ m^2 s Pa while that in case of MA at the same wt % was $3.12x10^{-10}$ g m/ m^2 s Pa, which is higher compared to composite films having citric acid. The tensile strength and percent elongation at break-point are, however, inferior compared to those for citric acid.

Citric acid with its three carboxyl groups is able to form more ester bonds with hydroxyl groups in PVA-BPF composite films Its effect is seen in the tensile tests as well as elongation and WVP tests (Reddy and Yang, 2010; Rojas and Azevedo, 2011). In view of above observations citric acid was selected as the second cross-linker.

The best formulation for PVA-BPF composite film therefore should have the PVA: BPF ratio of 80:20; 1 wt% glutaraldehyde, 10 wt% sorbitol and 10 wt% citric acid. The corresponding values of PVA-BPF composite films are: tensile strength = 38.3 MPa, percent elongation at break-point = 106.8 %, WVP = 2.62 x 10^{-10} g m/ m^2 s Pa, water contact angle = 71.4° and water swelling weight = 67.4%.

Biodegradability Test

Three identical samples PVA-BPF composite film prepared using above composition and simple PVA film were subjected to biodegradability test by burying under soil for 90 days as described in section 3.8.9 of chapter 3. Figure 4.15 shows the rate of biodegradation of PVA-BPF composite films as compared to PVA films. The films followed the general weight loss profile and not much difference was observed between the biodegradation rate of PVA and PVA-BPF composite films. Within the period of test, the PVA films were degraded by around 38.6 % while the PVA- BPF films degraded by around 62.3%. This was in part due to the BPF loading in composite films which is perfectly biodegradable. Similar profiles of PVA and composite biodegradation

has also been reported by (Maiti et al., 2012). Complete biodegradation of PVA films under soil burial has been reported by (Kumar et al., 2018; Ong et al., 2020) while (Cinelli et al., 2003) have shown Starch PVA and lignocellulosic films to biodegrade within 30 days in compost.

The biodegradation rates differ as per the microbial flora present in the soil samples. The soil used in this study was garden soil enriched with compost of cow dung and vermin-compost also being a garden soil it was very rich in organic matter. The sewage water used to add moisture to soil was also helpful in adding to the variety of microbial consortia and therefore the higher rate of degradation of PVA and PVA-BPF composite films could be achieved.

Table 4.5: Effect of citric and maleic acid (second cross-linker) amount on the tensile strength, percent elongation at break-point, water vapor permeation and water contact angle of PVA–BPF composite films

	Tensile strength (MPa)		**Elongation at breakpoint (%)**	
Wt%	**Citric Acid**	**Maleic Acid**	**Citric Acid**	**Maleic Acid**
0	30.8±1.8	30.8±1.8	68.93±14.2	68.93±14.2
5	35.4±3.1	32.8±2.7	91.11±9.5	101.11±16.7
10	**38.3±2.4**	33.7±3.4	**106.84±14.3**	126.84±15.4
15	33.4±2.5	35.3±3	113.82±13.9	133.82±10.6
20	31.8±3.6	29.6±4.1	135.28±13	145.28±13.2
25	28.7±3.2	25.3±1.3	172.53±12.1	182.53±8.2
	WVP ($x10^{-10}$g.m/m^2/s/Pa)		**Water contact angle (°)**	
Wt%	**Citric Acid**	**Maleic Acid**	**Citric Acid**	**Maleic Acid**
0	2.57±0.4	2.57±0.4	67.2	67.2
5	3.38±0.4	3.58±0.6	70.2	67.8
10	**2.62±0.3**	3.12±0.4	**71.4**	65.6
15	3.95±0.5	2.95±0.3	68.1	62.7
20	4.38±0.7	4.53±0.5	66.2	61.4
25	4.7±0.6	5.31±0.6	64.6	59.2

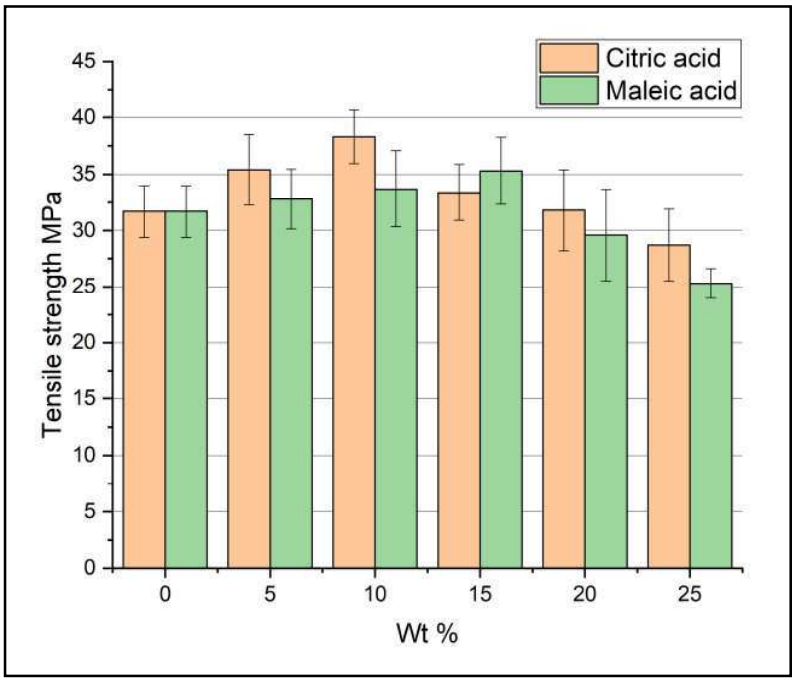

Figure 4.12: Variation of tensile strength of PVA-BPF composite films with concentrations of citric and maleic acids

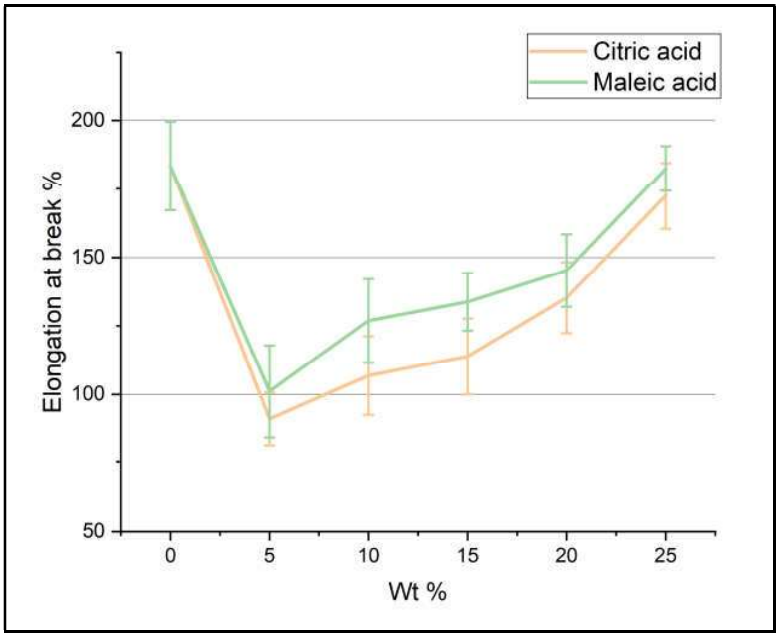

Figure 4.13: Variation of percent elongation at break-point of PVA-BPF composite films with concentration of citric and maleic acids

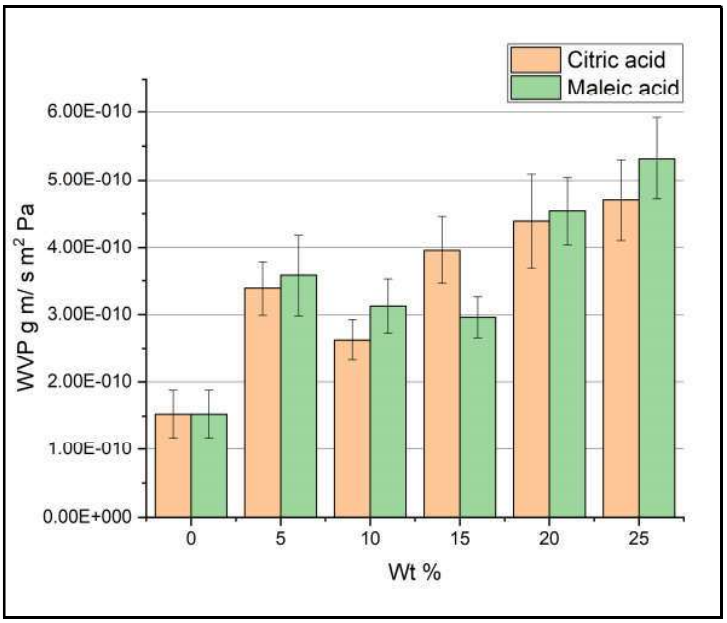

Figure 4.14: Variation of water vapor permeation rate through PVA-BPF composite films with concentrations of citric and maleic acids in film

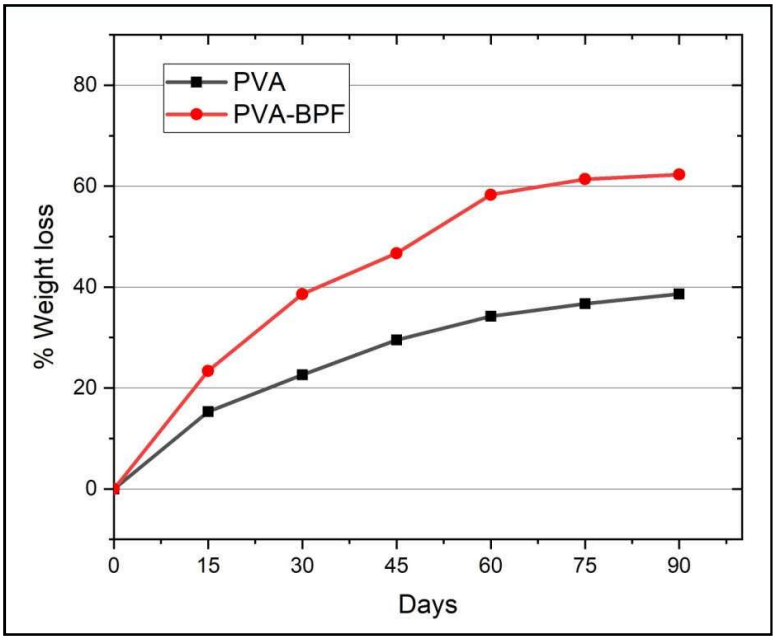

Figure 4.15: Comparison of the rate of biodegradation of PVA-BPF composite films and plain PVA films

4.2: Effect of acid and alkali treatment on Properties of PVA-tBPF composite films

The banana pseudo stem fibers of size <53 μm were treated with aqueous solutions of varying concentrations of Sulphuric acid (at 1, 2.5, 5, 7.5 and 10 %w/v) and alkali Sodium hydroxide (at 1, 2.5, 5, 7.5 and 10 % w/v) at temperature of 90°C (Section 3.3, Chapter 3). These fibres were then reinforced in PVA matrix to prepare composite films with PVA: BPF at 80:20 ratios. The effect of acid and alkali treatment on mechanical and water resistance properties of PVA-tBPF composite films was evaluated as described earlier (Section 3.8, Chapter 3).

4.2.1 SEM analysis of acid and alkali treated BPF

Figure **4.16** shows SEM micro-photographs of untreated and alkali and acid treated fibres of banana pseudostem of <53um size. As can be seen from the micrographs, the raw fiber is rough with globular particles attached to its outer surface while the alkali treated fibres show a relatively smoother surface morphology due to the removal of hemi-cellulose and lignin by the alkali covering the micro-fibrils (Prasad et al., 1983; Rahman and Khan, 2007; Valadez-Gonzalez et al., 1999) . Similarly the acid treatment of fibres has also resulted in smoothening of the outer surface of fibres due to the hydrolysis of exposed cellulose and hemicelluloses.

The alkali treatment also results in the formation of cellulose nano-crystals which can be seen as cylindrical nano-structures in **Fig. 4.16 (b).** Formation of such nano-crystals of cellulose have also been observed by (de Souza Lima and Borsali, 2004; My Ahmed Saïd Azizi Samir et al., 2004; Roohani et al., 2008) but their formation has always been attributed to the acid hydrolysis and never to the alkali treatment. The formation of such cylindrical rod shaped nano-crystal like structure takes place due to excessive removal

of lignin and hemicelluloses and the degradation of exposed amorphous cellulose by alkali at high temperature.

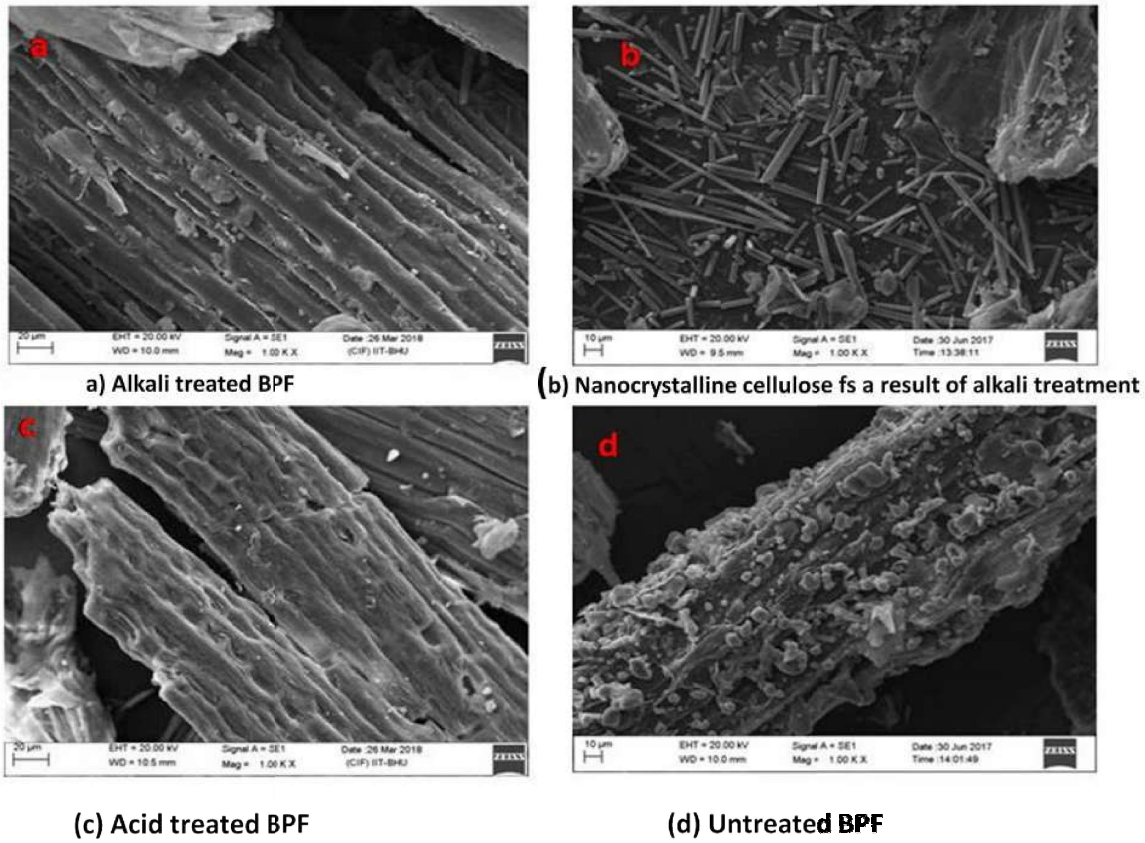

Figure 4.16 SEM Micrograph of (a) Alkali treated BPF; (b) Cylindrical nano crystalline cellulose as result of alkali treatment; (c) Acid treated BPF; & (d) untreated BPF

Table 4.6 Results of compositional analysis of alkali and acid treated fibres

Alkali treated	Lignin (%)	Cellulose (%)	Hemicellulose (%)
1 %	9.6	73	4.5
2.5%	11.2	68	5
5%	8.4	75	3.4
7.5%	6.5	78	2.5
10%	10.2	70	4.8
Acid treated	Lignin (%)	Cellulose (%)	Hemicellulose (%)
1%	8.5	72	4.8
2.5%	7.8	77	3.6
5%	7.2	80	3
7.5%	8.1	74	4.2
10%	9.2	69	5.2
Untreated	**13**	**65**	**6**

4.2.2 FTIR spectra and XRD patterns of acid and alkali treated fibres

The FTIR spectra and XRD finger prints of treated and untreated BPF were recorded to understand the effects of alkali and acid treatment on fibres particularly on their chemical groups and crystallinity. **Figures 4.17 (a)** and **(b)** show the FTIR spectra of alkali and acid treated fibres together with that for untreated fibres. **Figures 4.18 (a)** and **(b)** shows the XRD diffractogram of alkali and acid treated fibres together with the diffractogram for untreated fibres.

The FTIR spectra of BPF are characteristic of lignocellulosic biomass. The peaks at 3324 cm^{-1} are due to OH-groups and H-bonds between hydroxyl groups. Peaks at 2887-2918 cm^{-1} are due to vibrational stretching of C-H bonds in methyl and methylene groups in cellulose and hemicelluloses. The peaks at 1726, 1621, 1749 cm^{-1} are due to stretching of C=O bond of ketone/ carbonyl groups present in hemicellulose and lignin while they may also be due to pectins and waxes. The peaks between 1646 – 1261 cm^{-1} are due to vibrational stretching of C=C bonds of aromatic skeleton of lignin and CO adjacent to phenyl propene in lignin molecules (Corrales et al., 2007; Guimarães et al., 2009; Merlini et al., 2011; Yang et al., 2007).

As a result of alkali treatment the peaks at 1726 cm^{-1} are reduced significantly and also that at 1247cm^{-1} assigned to acetyl groups of hemicelluloses showed lower intensity as did the peaks between 3200-3500cm^{-1} indicating the removal of hemicelluloses and lignin. In case of acid treatment the hemicelluloses were removed to a lesser extent but the rest of the peaks followed a similar pattern showing the removal of lignin and hemicelluloses as a result of treatment.

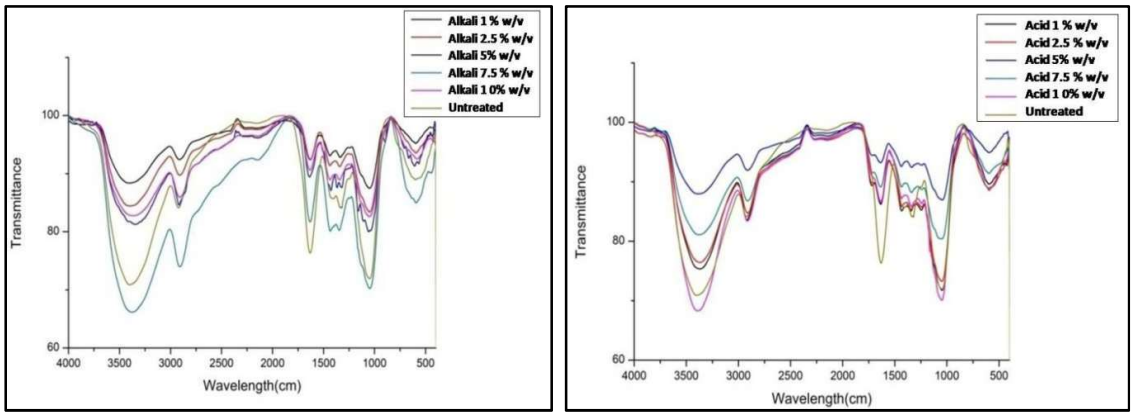

Fig. 4.17 (a) FTIR spectra of alkali treated fibres and (b) FTIR spectra of acid treated fibres

The XRD diffractogram (**Fig. 4.18 (a) and (b)**) of untreated fiber reveals peaks characteristic to lignocelluloses fibers with two peaks at 2θ degree values of 15 and 22° with the rest of the region being occupied by the amorphous particles. The diffractograms also show that due to acid and alkali treatment there is significant increase in the crystallinity as evident from intense peaks at 16 and 22° for acid treated and at 16, 22 and 35° for alkali treated fibres. This is attributed to the exposure of crystalline cellulose due to chemical treatments (Table 4.6). Further, there is not much difference in the peak intensities of fibres treated with different concentrations of alkali which suggests that treatment with 1% NaOH will also suffice for the suitability of fiber to be used in composite making. Higher intensities of peaks for 5% and 7.5 % acid treated fibres suggest that these concentrations and in particular the 5% acid will suffice for treatment. The results of compositional analysis of treated fibres as shown in **Table 4.6** also support this. As the concentration of alkali and acid is increased, there is a gradual increase in the removal of lignin and hemicelluloses resulting in an increase in the amount of cellulose in the treated fibres.

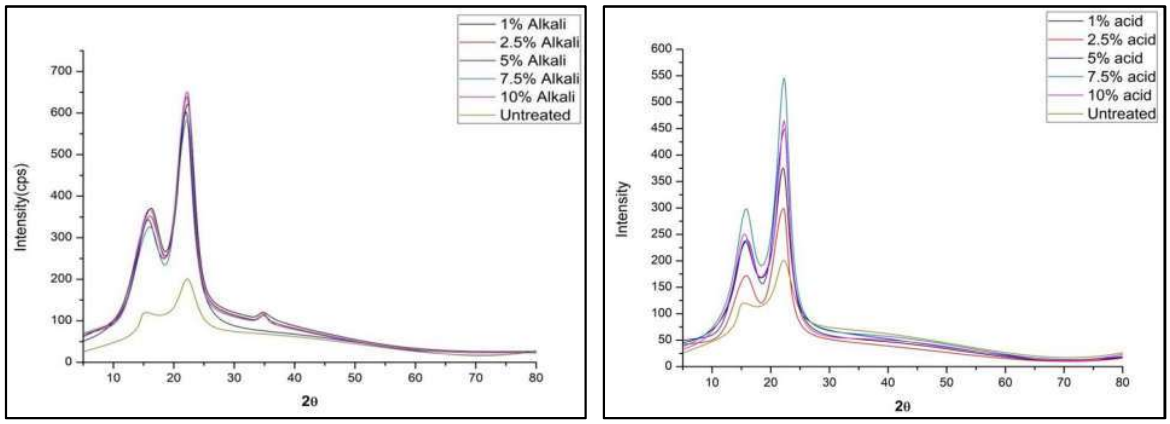

Fig. 4.18 (a) X-Ray diffractogram of alkali treated fibres and (b) X-Ray diffractogram of acid treated fibres

4.2.3 Water swelling test of PVA-tBPF composite films

The water absorption behavior of a film to be used for packaging purposes is an important characteristic. The water absorption behavior of composite films prepared using acid and alkali treated BPF was investigated as described in Section 3.8.6 of Chapter 3. The results obtained after every 24 hours up to 192 hours of experiments are plotted in **Figure 4.19(a)** for films prepared using alkali treated BPF and in **Figure 4.19(b)** for those prepared using acid treated fibers.

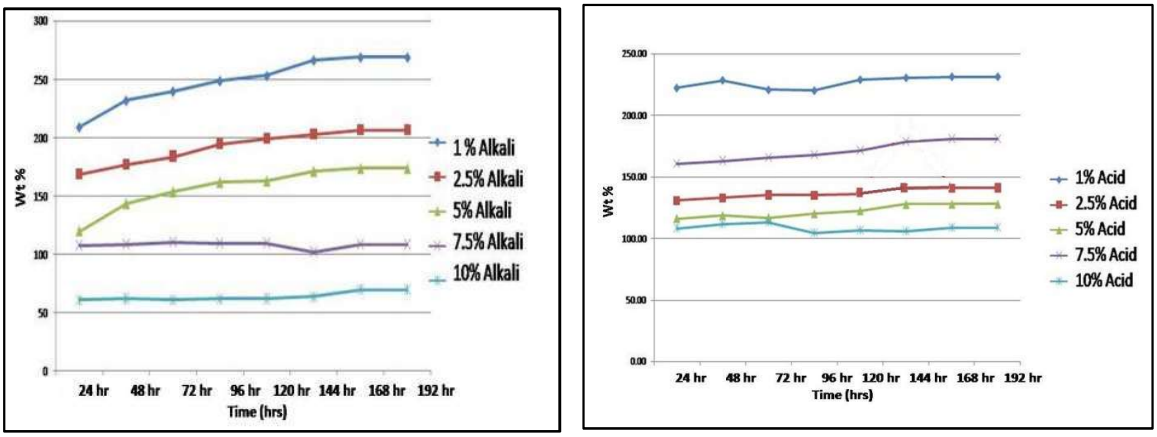

Fig 4.19: Swelling weight in water for (a) PVA-alkali treated fibres composite films and (b): PVA-acid treated fibres composite films

From the **fig. 4.19(a)** it can be seen that for alkali treated fibers swelling in water ranges from around 60 to more than 200 %. 10% NaOH treated fibers were most water uptake resistant and showed nearly constant weight gain after the first 24 hours. The films made using 1% NaOH treated BPF showed the maximum weight gain and the weight continued to increase for the next 5 days before reaching a constant weight. With regards to the packaging property of films, 10 % alkali treated fibers have desirable property of resistance to water uptake.

Fig. 4.19(b) shows the swelling in water for PVA composite films made using acid treated BPF. All the films showed weight gain in excess of more than 100 % with the least weight gain of 110% in case of 10% acid treated BPF. All the other films with fibers treated with lesser concentrations of acid had excessive weight gain. Acid treated films failed to be proved useful for film packaging.

Alkali treated films showed greater resistance to swelling in water due to enhanced hydrogen bonding between exposed cellulose and PVA matrix. The network structure formed by combining cross linkers and plasticizers with PVA and alkali treated BPF prevented the water molecules from dissolving and improved the water resistance of the uptake. Compared to other polymers that are frequently used, PVA being water soluble and hydrophilic possesses higher water uptake rate. The strong hydrogen bonding interactions between cellulose and PVA followed by cross linking would decrease the quantity of free OH groups, thus leading to a decrease in the moisture sensitivity of the composite films made using alkali treated fibers.

4.2.4 Tensile strength and percent elongation at break-point of PVA-tBPF composite films

Composite films of PVA and treated BPF were tested for their mechanical properties viz. tensile strength and percent elongation at break-point. **Figure 4.20 (a)** and **(b)** show

the results for tensile strength and elongation at break-point for both alkali and acid treated fibres respectively.

As can be seen from the graph, as the strength of alkali used to treat the fibres is increased, the tensile strength and percent elongation at break-point of composite films gradually increases while for the similar increase in acid concentration used to treat the fibres, the tensile strength and percent elongation at break-point of composite films gradually decreases. These results indicate that alkali treatment somehow favours the matrix – fiber interactions while acid treatment reduces the natural affinity between PVA matrix and acid treated fiber. XRD diffractogram for alkali treatment fibers shows exposure of cellulose upon treatment which readily forms hydrogen bonding networks. These internetworked hydrogen bond result in higher tensile strength and the tensile strength increases as more cellulose is exposed due to higher concentration of alkali used.

For alkali treated fibres, the tensile strength increases to 38.9 MPa for 1% alkali treatment and increases up to 44.3 MPa at 10 % alkali treatment. Percent elongation at break-point also increases from 109.7 % to 125.6 %. In the case of acid treated fibres, the acid treatment degrades the cellulose and the films show lower tensile strength as concentration of acid used for treatment is increased. With the acid treated fibres, tensile strength drops from 32.6 MPa at 1 % acid treated fiber to as low as 27.8 MPa for 10% acid treated fibres. Percent elongation at break-point decreases from 98.4% to 54.7 %.

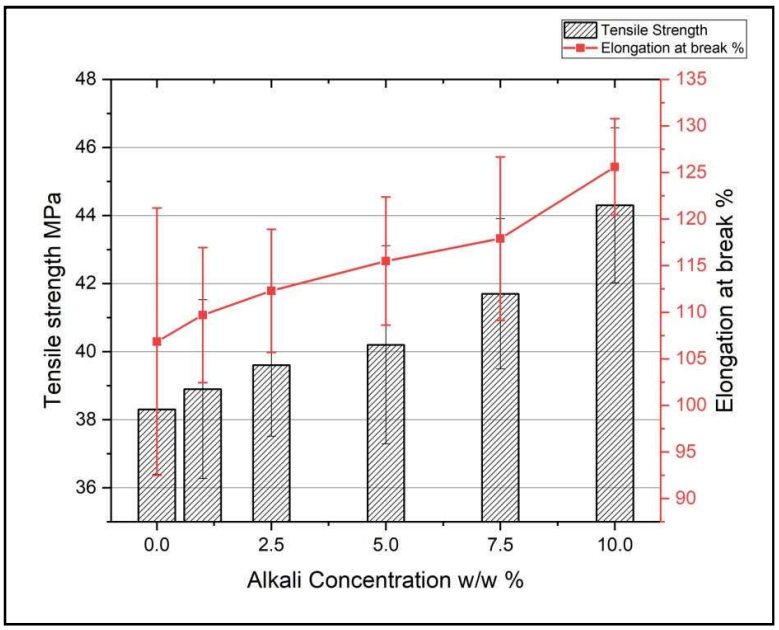

Fig. 4.20 (a) Tensile strength and percent elongation at break-point of alkali treated BPF-PVA composite films

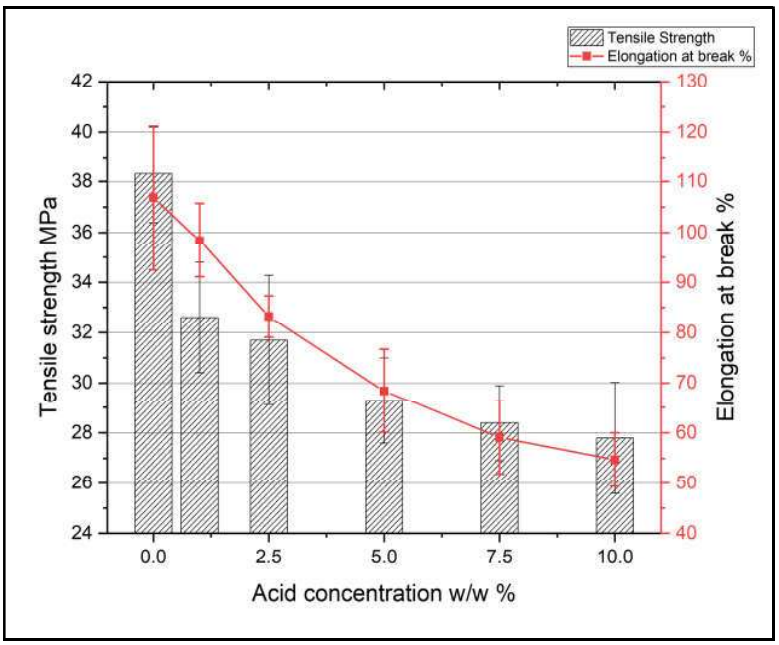

Fig. 4.20 (b) Tensile strength and percent elongation at break-point of acid treated BPF-PVA composite films

4.2.5 Water Vapour Permeability of PVA-tBPF composite films

Figure 4.21 shows the graph of WVP values for alkali and acid treated fibres – PVA composite films. WVP also follows the same pattern as seen for tensile strength. The WVP for alkali treated films increases as alkali strength used for treatment is increased and for 10 % alkali treated BPF composite films, WVP values of 2.14×10^{-10} g m /m^2 s Pa are seen. This further proves that alkali treatment gradually increases the matrix – fiber interaction. In the case of acid treatment, WVP values show a decreasing trend for increasing acid strength again hinting towards the fact that somehow Matrix- fiber interaction is being hampered possibly due to acid degradation of exposed cellulose. The acid treated films have very poor characteristics and cannot be used for packaging purpose while alkali treated films have better mechanical and water resistance properties.

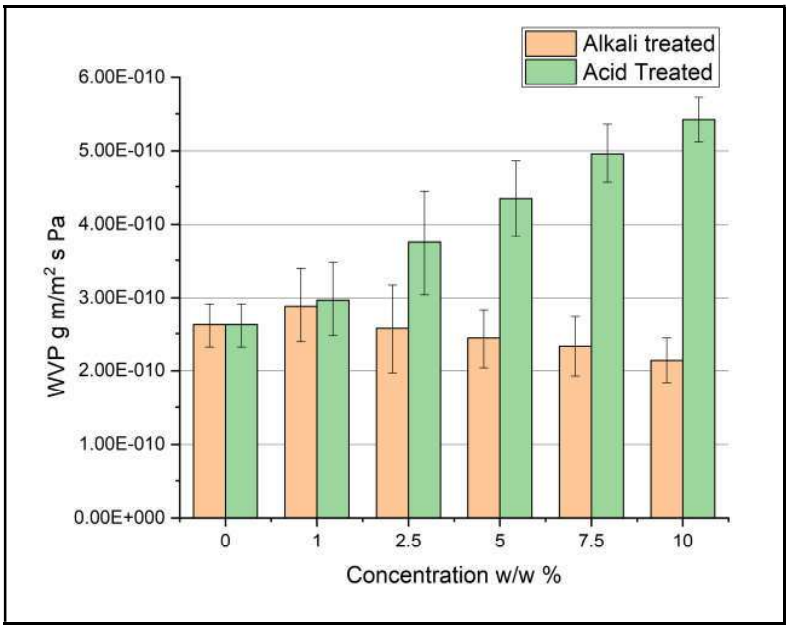

Fig. 4.21 Water vapour permeability of acid and alkali treated BPF – PVA composite films

4.3 Effect of nano-cellulose reinforcement on properties of PVA-BPF composite films

In order to further improve the mechanical and water resistant properties of PVA-BPF composite films nano-crystalline cellulose derived from microcrystalline cellulose has been used as the filler. The relevant characteristics of these films were evaluated in order to judge their suitability for packaging purpose. The results of these experiments are presented and discussed in this section.

4.3.1 Nano-cellulose synthesis and characterisation.

As described in Section 3.4 of Chapter 3, the nano-crystalline cellulose was prepared by dissolving micro-crystalline cellulose in a solution of NaOH and urea solution and precipitating the cellulose out as nano-particles by adding excess water. The size variation of these particles was evaluated using the dynamic light scattering (DLS) method. The DLS analysis showed the particle size varies in the range of 100 to 500 nm with average particle diameter of 254.8 ± 21 nm. The DLS method gives hydrodynamic diameter rather than the actual diameter and is usually greater than the actual diameter (Pandey et al., 2020).

The XRD difractograms for nano-cellulose and micro-crystalline cellulose are shown in **Fig. 4.23**. From this figure it is seen that for micro-crystalline cellulose there are three peaks at around 2θ = 22.6, 16.2, and 34.5 corresponding to (2 0 0), (1 1 0), and (4 0 0) lattice planes, respectively, the characteristic of cellulose I structure (Yu et al., 2014). In case of nano-crystalline cellulose the characteristic crystalline peaks are observed at 2θ = 12.03 and 22.5 for the (1 1 0) and (2 0 0) lattice planes, respectively, which is a characteristic of cellulose II structure (Yu et al., 2014). It is seen that micro-crystalline (MCC) and nano-crystalline cellulose (NCC) both exhibit a strong and sharp peak at around 2 θ = 22° which corresponds to (200) crystalline plane of cellulose I. (Z. Wang

et al., 2018). The broader peak at 22.6° for NCC compared to MCC indicates that the crystallite size of NCC is smaller than that of the MCC. As apart from the peak width no other changes are observed in the two diffractograms suggesting that the nano-cellulose crystallite structure has not changed (Shankar and Rhim, 2016). Urea is reported to decrease the crystallinity without interacting with the cellulose during the dissolution process (Isobe et al., 2013). Similarly reduced crystallinity and crystallite size have been observed when cellulose is treated with high concentration (7%,w/v) of NaOH (Mittal et al., 2011).

The FTIR spectra of MCC and NCC are shown in **Fig. 4.22**. It is seen that almost identical peaks are observed in both cases which are the characteristics of cellulose. The strong absorption OH stretching in the range of 3600–3000 cm^{1}, CH and CH_2 stretching vibrations between 3000 and 2800 cm^{1} and CO and CC stretching bands in the range of 1200–900 cm^{1} are the characteristic peaks for cellulose. The peaks at 1040 and 1044 cm^{1} for MCC and NC are due to the stretching vibrations of primary hydroxyl group of cellulose (Langkilde and Svantesson, 1995) and the peaks at 1344 and 1346 cm^{1} in MCC and NC are attributed to the bending vibration of COH (Maréchal and Chanzy, 2000) associated with the crystalline regions of cellulose (Åkerholm et al., 2004; Poletto et al., 2014). The peaks at 1646 and 1648 cm^{1} in MCC and NC correspond to –OH bending vibrations of absorbed water which is common in cellulose samples due to their hydrophillicity. The change in crystal structure of cellulose results in the disappearance or change in the intensity of certain peaks (Adsul et al., 2012) as the peak at 1430 cm^{1} associated with CH_2 bending vibration correspond to the "crystallinity band" in the cellulose (Shankar and Rhim, 2016). The decrease in the intensity of the peak at 1430 cm^{1} in case of NCC compared to MCC indicates decrease in the cellulose crystallinity during the preparation of nanocellulose.

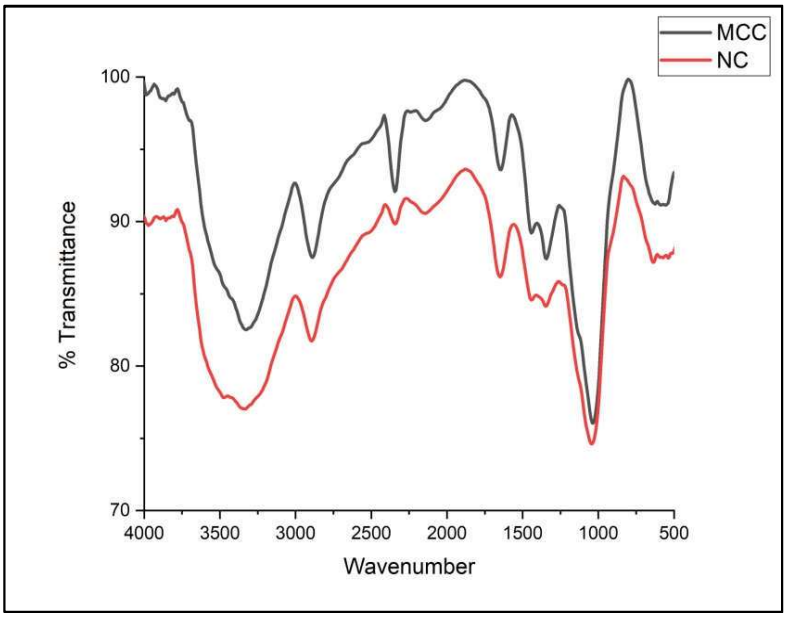

Figure 4.22 FTIR spectra of micro-crystalline cellulose and nano-cellulose

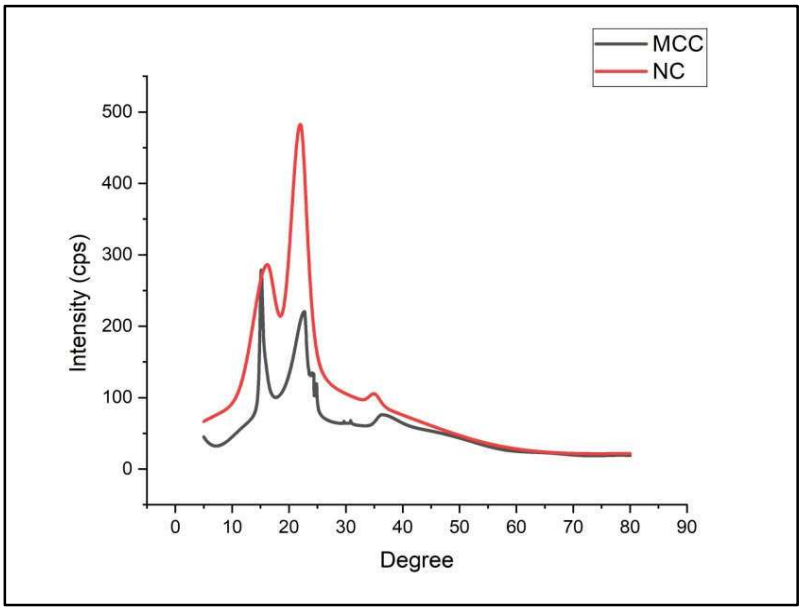

Figure 4.23 XRD diffractograms of micro-crystalline cellulose and nano-cellulose

4.3.2 Mechanical properties of PVA – BPF - NC composite films

Results of variation of tensile strength, percent elongation at break-point, WVP, extent of swelling and water contact angle with wt% of nano-cellulose are presented in **Table 4.7**. It is seen that addition of nano-cellulose particles has affected all the five parameters appreciably. The tensile strength has increased gradually with up to 3 wt% loading of nano-cellulose but has decreased appreciably with addition of 5 wt% nano-cellulose. The percent elongation at break-point similarly follows the same trend as tensile strength. The lowest value has been obtained with 5 wt% loading.

The improvement in properties of PVA films due to addition of NC has been attributed to the reinforcing effect of NC. Addition of NC increases the interfacial adhesion between the polymer matrix and BPF particles due to the presence of multiple hydroxyl groups thus allowing the transfer of load from polymer chains of the matrix to BPF particles through NC fibres (Dufresne et al., 2009). These hydroxyl groups develop a network of intermeshed framework resulting in higher tensile strength and percent elongation at break-point (Frone et al., 2011). However at higher concentrations of nanocellulose the films lose tensile strength due to non homogenisation of nanocellulose in the film forming solution. Others have also reported that at higher concentrations the stronger interfacial adhesions may decrease % elongation at break-point causing the films to be less flexible (Cheng et al., 2014; Roohani et al., 2008; Zhou et al., 2012). **Figure 4.24** depicts the variation of tensile strength and % elongation at the break-point. The reduction in tensile strength and elongation at break of films with 5 wt% NC is direct result of non homogenised films with microscopic clusters of agglomerated NC (Liu et al., 2013; Luzi et al., 2017). These agglomerates are unable to withhold load bearing due to lesser hydrogen bonding interactions with the polymer matrix and give way in presence of external load (Pereira et al., 2014).

Table 4.7 Effect of nanocellulose loading on tensile strength, % elongation at break-point, water vapor permeation and water contact angle of PVA-BPF composite films reinforced with nano-cellulose

Composite Film	Tensile Strength (MPa)	Elongation at Break-point (%)	WVP ($x10^{-10}$g.m / m^2.s. Pa)	Water Swelling (%)	Contact Angle (°)
PVA	31.7±2.3	183.4±16.1	2.57±0.4	--	65.8
PVA-BPF	38.3±2.4	**106.84±14.3**	2.62±0.3	67.4±2	71.4
PVA-BPF-NC 0.1	39.2±2.4	122.1±12.6	2.23±0.4	42.3±1.9	74.8
PVA-BPF-NC 0.5	41.5±2.8	129.1±7.1	2.14±0.5	32.4±2.2	77.3
PVA-BPF-NC 1	42.6±2.7	127.8±14.4	2.07±0.4	27.6±1.7	79.6
PVA-BPF-NC 3	43.8±3.6	139.5±12.5	1.84±0.3	16.8±2.4	80.2
PVA-BPF-NC 5	28.7±3.4	87.4±9.2	1.14±0.2	49.7±2	82.7

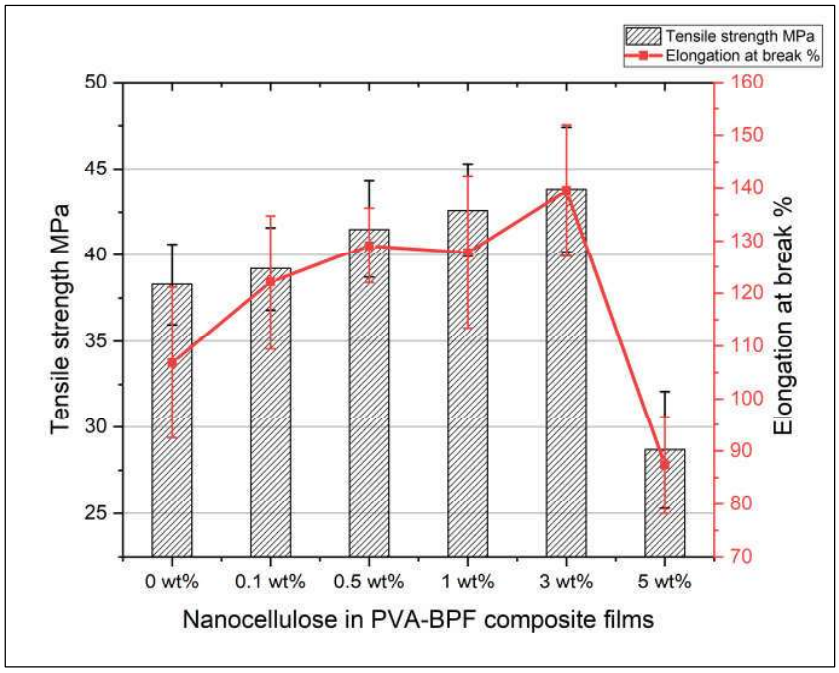

Figure 4.24 Effect of nanocellulose loading on tensile strength and %elongation at break-point of nano-cellulose reinforced PVA-BPF composite films

4.3.3 Water swelling test, water vapour permeability and contact angle tests of PVA – BPF NC composite films

Swelling in water

The PVA films dissolved within 6 hours after immersion in distilled water at room temperature. However the addition of BPF in the composite films along with cross

linkers and plasticizers improved the resistance to dissolution and films showed only 67.4 % swelling after the initial 24 hours. This is due to the formation interlocking bonds between the hydroxyl groups of BPF and PVA and the film preparation process (Srivastava et al., 2019). As seen from **fig. 4.25**, a substantial reduction in swelling has resulted through the incorporation of NC and the % swelling as low as 16.8% was observed for 3 wt% NC. The interfacial interaction between NC, PVA and BPF through extensive hydrogen bonding is the main reason behind this improvement in the % swelling. The reduction in the WVP values also increased and 3wt% NC loaded PVA-BPF-NC composite film exhibited the maximum reduction in WVP. **Fig. 4.26** shows the effect of nano-cellulose addition on the water swelling behaviour of films. Here again the extent of swelling is directly dependent upon the percentage of neon-cellulose added to the film casting solution up to 3 wt % Nanocellulose loading after which there is sudden increase in water swelling which may be attributed to the high level of agglomeration of nanocellulose within the films and the resulting non homogenous dispersion of Nanocellulose within the film structure causing whole sections of films to be susceptible to swelling.

Contact angle

The contact angle increased significantly too. It has been reported that incorporation of NC in composite films leads to the filling of gaps between the polymer chains as well as BPF by NC thereby increasing the tortuosity of the film and restricting page of water molecules (Azeredo et al., 2012; Chen et al., 2012). Surface hydrophillicity is also reduced and 5wt% NC loaded films had the greatest reduction in hydrophillicity (water contact angle = 82.7°) due to the cross-linked network created by hydrogen bonded NCs.

Water vapour permeability

From **Fig. 4.25** it is seen that as the reinforcement of nanocellulose in the PVA-BPF composite films increases, the water vapour permeation decreases consistently from 2.62 $x10^{-10}$ (g.m / m^2.s. Pa) for PVA-BPF film to 1.14$x10^{-10}$ (g.m / m^2.s. Pa) for PVA-BPF-NC film with 5 wt% nano-cellulose loading. It is interesting to note that PVA-BPF-NC composite films had WVP values 2 orders of magnitude lower than agar composite films (Shankar and Rhim, 2016). It has been reported that Nanocellulose fill the gap within film matrix and increase the tortuosity for water molecules to pass through (Azeredo et al., 2012; Chen et al., 2012)

From the above results it can be inferred that nano-cellulose reinforced PVA-BPF composite films are superior to PVA films or PVA-BPF composite films.

4.3.4 Biodegradability of PVA-BPF-Nanocellulose composite films

Figure 4.27 presents the weight loss curves for PVA, PVA-BPF and PVA-BPF-NC composite films. It is seen that Nanocellulose incorporated PVA-BPF composite films show slower degradation than PVA-BPF films. While PVA-BPF films degraded up to 62.3 % in 90 days, the PVA-BPF-Nanocellulose films showed 54.8 % degradation. Nanocellulose incorporation creates hydrogen bonded network within the film structure and due to these hydrogen bonding and the resulting resistance to water swelling the degradation rates are less as compared to PVA-BPF composite films. The biodegradation of composite films in soil burial takes place in two steps, first the composite film swell by diffusion of water molecules which allow microbes to thrive over films and secondly, the films structures are degrade as a result of enzyme action from enzymes released by microbes (Abdullah et al., 2017; Guohua et al., 2006). The biodegradability therefore is affected by water resistance of composite films.

Biodegradability and weight loss have been reported to decrease in the presence of nanofillers (Taghizadeh et al., 2013).

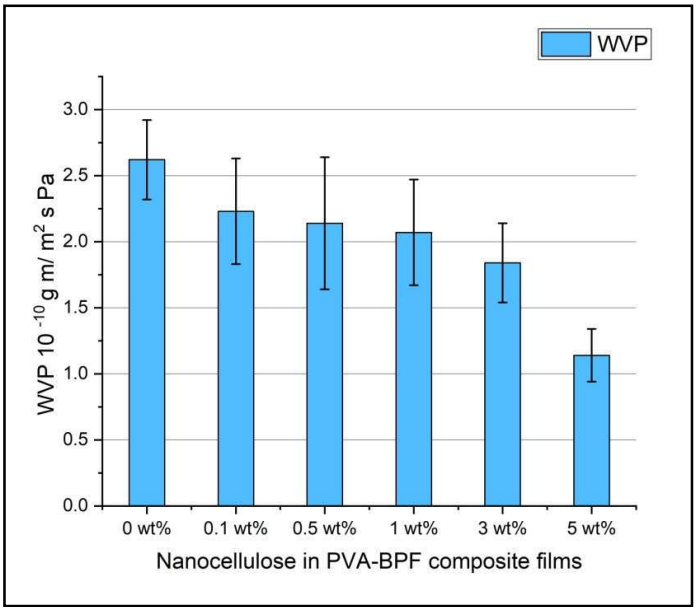

Figure 4.25 Effect of nanocellulose on water vapor permeation of nano-cellulose reinforced PVA-BPF composite films

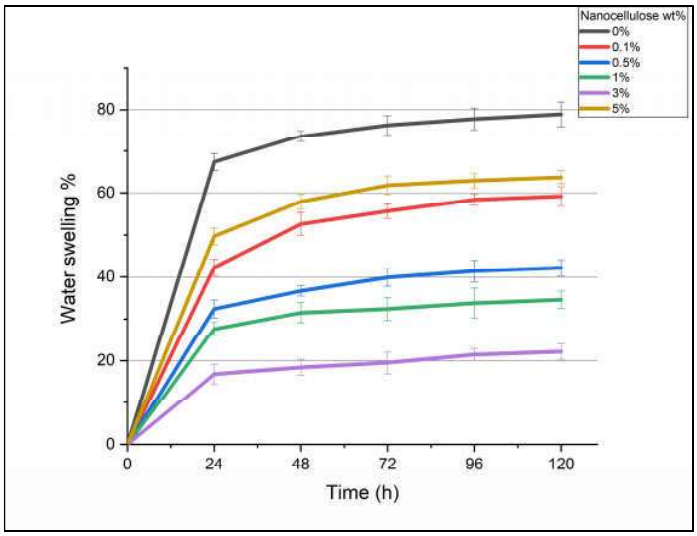

Figure 4.26 Effect of nanocellulose percentage on water swelling behavior of nano-cellulose reinforced PVA-BPF composite films

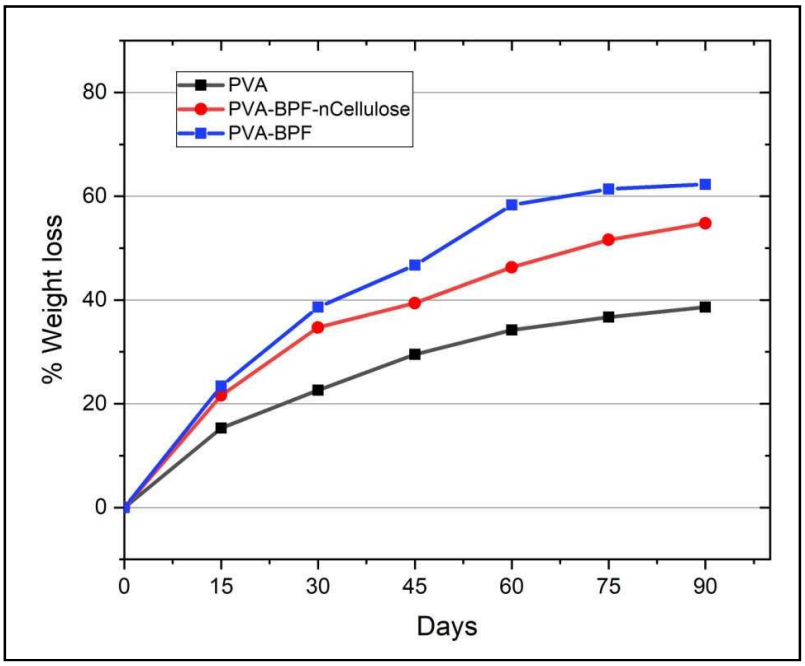

Figure 4.27 Comparison of biodegradation of PVA, PVA-BPF and nanocellulose reinforced PVA-BPF composite films

4.4 Effect of nano-clay and citric acid modified nano-clay reinforcement on properties of PVA-BPF composite films

Montmorillonite – Sodium (MMT-Na) nanoclay is hydrophilic nanoclay known for its compatibility with hydrophilic polymers like PVA. Nanoclay (MMT) and citric acid modified nano-clay (CMMT) was added to PVA-BPF films to see its effect on mechanical and barrier properties of composite films. This section discusses the results obtained after reinforcing PVA-BPF composite films with nano-clay and citric acid modified nano-clay.

4.4.1 Citric acid modification of nano-clay

The nano-clay, Na-MMT was modified by citric acid as explained in section 3.6 of Chapter 3. Figure 4.28 presents the FTIR spectra of MMT and CMMT (Citric acid modified MMT) nano-clay. MMT exhibits the four types of vibrations for Si–O and OH bonds at 467, 525, 918, 3626, 1040 and 1635 cm-1 which has been reported by (Azizi et al., 2010; Koosha et al., 2015). Citric acid modification of MMT is evidenced by the peaks characteristic for CMMT at 3428 and 3620, 2933, 1643, 466 and 520 cm 1 which are attributed to OH stretching, CH stretching, OH bending and Si–O bending, respectively (Navarchian et al., 2015; Pirooz et al., 2018). **Figure 4.29** shows the XRD diffractogram for MMT and CMMT. As can be seen from the WA X-ray diffractograms of MMT and CMMT, untreated MMT shows a characteristic peak at 2θ angle 7.26° corresponding to d-spacing of 1.22 nm. Treatment with citric acid causes a shift in the peak to 2θ angle 5.62° corresponding to d-spacing of 1.57 nm. As observed by Majdzadeh-Ardakani et al. (2010), “the citric acid molecules penetrate into the interlayer space and replace sodium cations thereby enlarging gallery spacing and shifting the peak position to a lower angle in the XRD pattern. The citric acid molecules act as a link between the clay and PVA, BPF, through H-bonding leading to a very efficient intercalation process”.

Table 4.8 Effect of MMT and CMMT loading on tensile strength, % elongation at break-point, water vapor permeability, water contact angle and water swelling of PVA-BPF composite films reinforced with nanoclay

Composite Film	Tensile Strength (MPa)	Elongation at Break-point (%)	WVP ($x10^{-10}$g.m / m^2.s. Pa)	Contact Angle (°)	Water Swelling (%)
PVA	31.7±2.3	183.4±16.1	2.57±0.4	--	65.8
PVA-BPF	38.3±2.4	106.84±14.3	2.62±0.3	56.7	71.4
PVA-BPF-MMT 1	40.7±3.7	116.8±12.6	2.14±0.4	29.8	73.2
PVA-BPF-MMT 3	42.7±2.6	134.7±11.5	1.92±0.3	14.3	75.8
PVA-BPF-MMT 5	32.4±1.5	79.2±11.9	2.54±0.3	43.2	79.7
PVA-BPF-CMMT 1	41.9±3.2	126.3±15.2	1.96±0.4	27.5	74.6
PVA-BPF-CMMT 3	44.6±3.5	135.7±9	1.87±0.3	13.6	79.1
PVA-BPF-CMMT 5	29.4±2.9	81.5±13.7	2.23±0.4	41.3	82.4

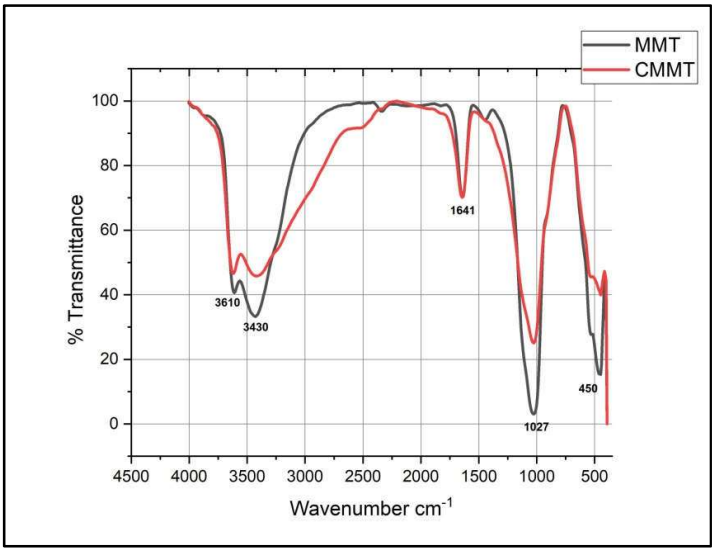

Fig. 4.28: FTIR spectra of Montmorillonite and Citric acid modified Montmorillonite

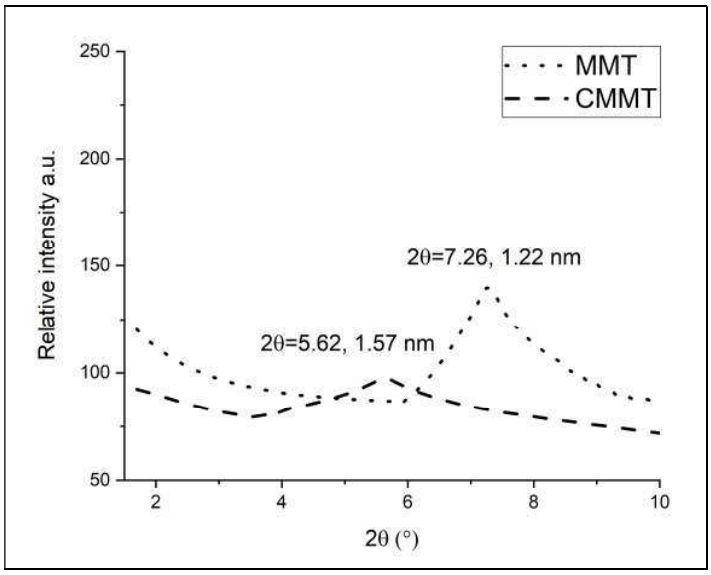

Fig. 4.29: X-Ray Diffractogram of Montmorillonite and Citric acid modified Montmorillonite

4.4.2 Mechanical properties of MMT and CMMT reinforced composite films

In PVA-BPF-MMT and PVA-BPF-CMMT composite films, the sodium cation or citric acid molecule provide interfacial interactions with both PVA matrix and BPF filler and results in improved exfoliation of nano-clay (Dean et al., 2007) thereby improving the mechanical properties of the composites (Huang et al., 2006).

Table 4.8 lists the values for tensile strength and elongation at break-point % for MMT and CMMT reinforced PVA-BPF composite films. As can be seen from **Table 4.8** and in the **figure 4.30** and **fig. 4.31**, nanoclay incorporation into the composite films in treated and untreated forms improves the tensile strength as well as % elongation at break-point when nano-clay is up to 3 wt %. Tensile strengths and % elongation at break-point are found to be 42.7 MPa and 134.7% and 44.6 MPa and 135.7% for MMT and CMMT incorporated composite films respectively.

H-bonding interaction between hydrated sodium cation in MMT with the free OH groups of the BPF and PVA chains could facilitate the dispersion of clay platelets throughout the composite matrix. Similarly CMMT shows slightly better results than

MMT as the interaction between citric acid modifier groups of CMMT and hydroxyl groups of PVA-BPF matrix facilitates dispersion of clay platelets throughout the composite matrix. This improves exfoliation of clay platelets and thus improvement in tensile strength and % elongation at break-point is seen (Dean et al., 2007). Since there is greater chemical interaction between citric acid and PVA-BPF matrix and Since CMMT has wider gallery spacing allowing for better intercalation of PVA chains – BPF particles, CMMT incorporation provides better improvements in mechanical properties. (Chenwei et al., 2018b; Majdzadeh-Ardakani and Nazari, 2010; W. Wang et al., 2018)

However, at 5 wt % clay loading the tensile strength and % elongation at break-point reduces 32.4 MPa and 79.2% in case of MMT and 29.4 MPa and 81.5% in case of CMMT. Higher concentration of nano-clay in the composite films (>3 wt% in our case) results in abrupt failure of composite films in mechanical testing. Such abrupt failure is due to the possible agglomeration of nano-clay particles into matrix resulting from non homogenous distribution. These agglomerates are formed when the clay layers cannot be further exfoliated/ intercalated within the matrix (Majdzadeh-Ardakani et al., 2010). Possible reason for such agglomeration may be lack of proper homogenization when preparing films by solution casting as the mixture is viscous due to presence of PVA and BPF. Saturation may also be achieved at higher loading of nanoclay.

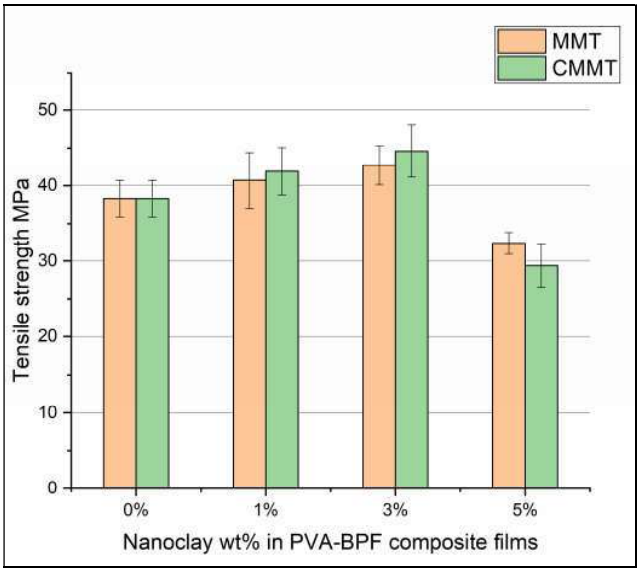

Fig. 4.30: Variation of Tensile strength of PVA composite films incorporated with Montmorillonite and Citric acid modified Montmorillonite

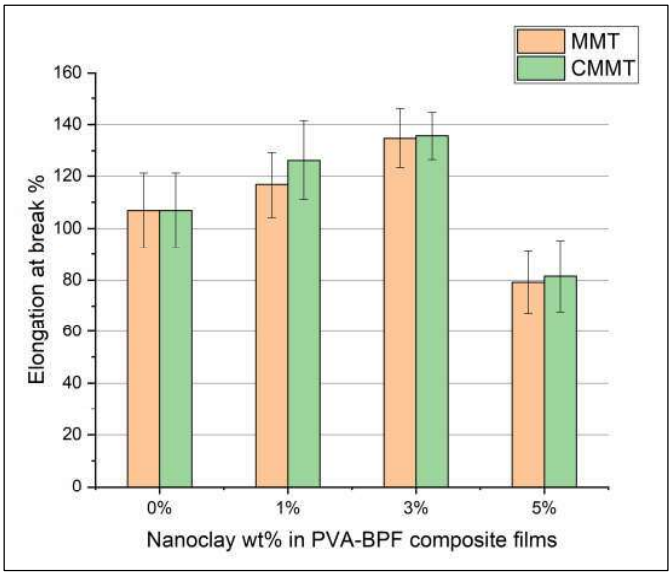

Fig. 4.31: Variation of elongation at break-point of PVA composite films incorporated with Montmorillonite and Citric acid modified Montmorillonite

4.4.3 Water swelling test, water vapour permeability and contact angle tests of PVA – BPF- MMT and PVA-BPF-CMMT composite films

Nano-clay has long been used for improvements of barrier properties of composite films. **Figure 4.32** shows the variation of WVP of PVA-BPF composite films incorporated with MMT and CMMT. The addition of MMT and CMMT nano-clay at 1 and 3 wt% loading gradually lower the WVP values of composite films and as in the case for mechanical properties. At 3 wt% loading the WVP values are found to be 1.92 x 10^{-10} g m/ m^2 s Pa and 1.87x 10^{-10} g m/ m^2 s Pa for MMT and CMMT incorporated composite films respectively. Swelling in water also improves significantly and 3 wt% CMMT loaded films show only 13.6% swelling in water and water contact angle improves to 79.1°.

The reason for such improvements in water barrier is the exfoliation of clay platelets in the PVA-BPF matrix. This increases the tortuosity for water molecules to pass through which depend on first their solubility in the film and later their diffusion across the composite to pass through the composite film (Han, 2005). At higher loading (>3 wt%) the films show slightly higher values of WVP which may be attributed to agglomeration of clay platelets and therefore the values of WVP are similar to those of PVA-BPF composite films.

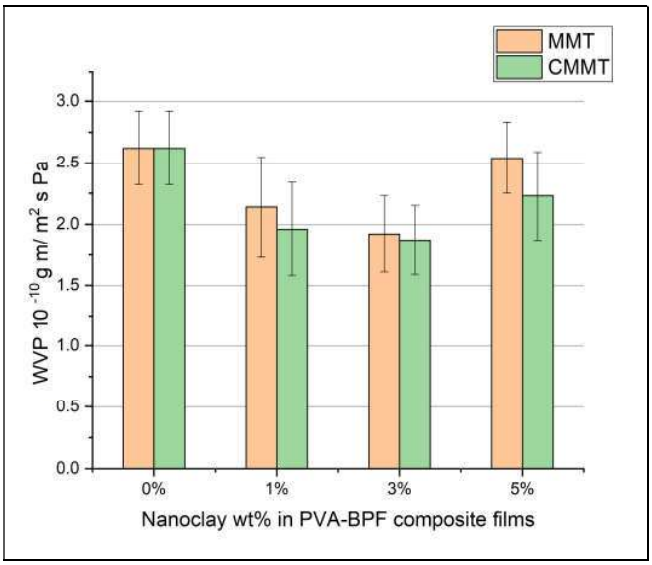

Fig. 4.32: Variation of water vapour permeability of PVA composite films incorporated with MMT and CMMT

4.4.4 Biodegradability of PVA-BPF-MMT and PVA-BPF-CMMT composite films

As seen from **fig. 4.33**, PVA-BPF composite films reinforced with MMT and CMMT show similar biodegradation profiles to PVA-BPF composite films.

PVA –BPF films show 62.3% weight loss while PVA-BPF composites reinforced with MMT and CMMT show weight loss of 55.9% and 51.4% respectively.

It has been reported that nanofillers usually decrease the rate of degradation (Taghizadeh et al., 2013) however is has also been reported that nano-clay, particularly hydrophilic nano-clay like MMT promote the degradation due to their hydrophilic nature (Abdullah et al., 2017). However at higher concentrations the degradation rates are lowered. The rate of degradation of MMT reinforced composite films is higher than CMMT reinforced composite films as the CMMT nano-clay is citric acid functionalised and therefore exhibit chemical interaction with the PVA-BPF matrix. This interaction which helps improve mechanical and barrier properties also hinders the swellability of composites thereby lowering degradation rates.

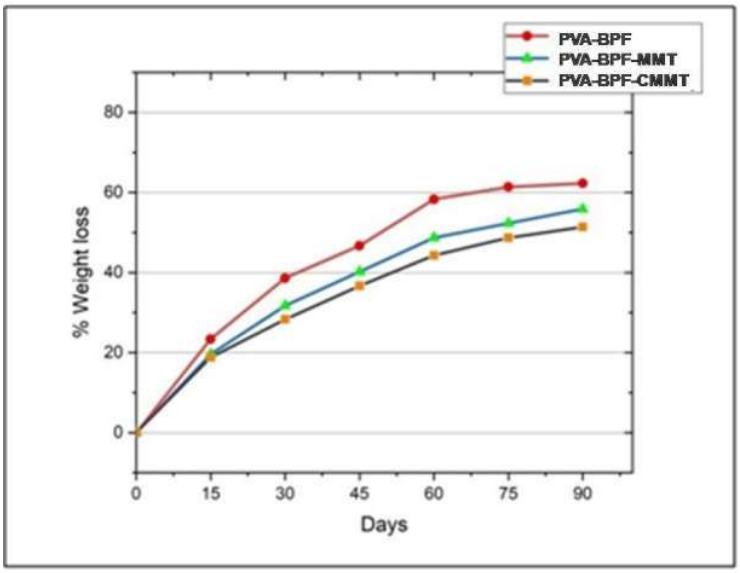

Fig. 4.33: Comparison of biodegradation of PVA-BPF and PVA-BPF composite films reinforced with MMT and CMMT